Eur. Phys. J. D **39**, 433–438 (2006)
DOI: 10.1140/epjd/e2006-00123-2

THE EUROPEAN PHYSICAL JOURNAL D

Three-dimensional growth characteristics of antimony aggregates on graphite

S.A. Scott[1] and S.A. Brown[1,a]

The MacDiarmid Institute for Advanced Materials and Nanotechnology, Department of Physics and Astronomy, University of Canterbury, Christchurch, New Zealand

Received 10 January 2006
Published online 13 June 2006 –

Abstract. The growth of antimony aggregates on the basal plane of graphite via diffusion and aggregation of Sb_4 clusters has been investigated with scanning electron microscopy, and in 3-dimensions with atomic force microscopy. The aggregate morphologies depend critically on the deposition conditions. It is shown that a transition from compact to branched morphologies with increasing aggregate size, depends on the particle flux. Also, the aggregate heights are strongly influenced by flux, with higher fluxes producing flatter aggregates. The heights of individual island branches are also shown to depend on the local diffusion field.

PACS. 68.43.Jk Diffusion of adsorbates, kinetics of coarsening and aggregation – 61.46.-w Nanoscale materials – 81.16.Dn Self-assembly

1 Introduction

Spontaneous pattern formation in thin film growth has attracted much attention in recent years, due to its potential for providing a method for self-assembling nanostructures with tailored morphologies [1].

The nucleation and growth of thin films from the vapor phase generally occurs in a non-equilibrium environment. When particles are deposited on atomically flat and weakly interacting surfaces, they diffuse until they collide with other diffusing particles (or defect traps) and nucleate islands [2]. A thermodynamic tendency to minimize the free energy of these islands, favors aggregation of compact structures. However, the kinetics of diffusion of particles to the growth front often drives the system towards dendritic and irregular shapes [1]. Manipulating the balance between these two competing processes allows a degree of control over the island morphologies, and consequently the opportunity to self-assemble well defined nanostructures on surfaces.

The diffusion and aggregation of antimony on graphite surfaces has produced some striking examples of pattern formation in a non-equilibrium system [3–6]. However, systematic investigations of the dependence of morphology on the growth environment in this system, has been limited to 2-dimensional studies, predominantly with scanning electron microscopy (SEM) and transmission electron microscopy. We report here on the flux dependence of a cross-over from compact to branched morphologies, and extend the previous studies to 3-dimensions by performing an atomic force microscopy (AFM) study of the effect of the growth conditions on the island heights.

2 Experiment

Samples were prepared by vapor deposition in an ultrahigh vacuum (UHV) chamber. Grade STM-2 HOPG substrates (SPI supplies) were cleaved in air with adhesive tape, and immediately loaded into the UHV chamber. Residual surface contaminants were removed by thermal treatment under UHV at ∼720 K, for at least 12 h in a heat shielded radiative oven, powered with a 50 W lamp. High purity (99.998%) Sb was evaporated from a crucible, and deposited on the basal plane of HOPG at room temperature, with the particle flux, F and coverage, θ monitored with a calibrated quartz crystal microbalance. Thermal evaporation of antimony is known to produce a vapor comprised exclusively of Sb_4 particles [7]. The coverage is measured in units of monolayers (ML) where 1 ML is arbitrarily defined as the average inter-atomic distance in bulk antimony (3.1 Å) Samples were prepared for the flux range 0.005–2.0 Å/s and coverages between 2 ML and 40 ML. The chamber was vented with dry nitrogen one hour after deposition and the samples removed for ex situ analysis with SEM and AFM.

[a] e-mail: simon.brown@canterbury.ac.nz

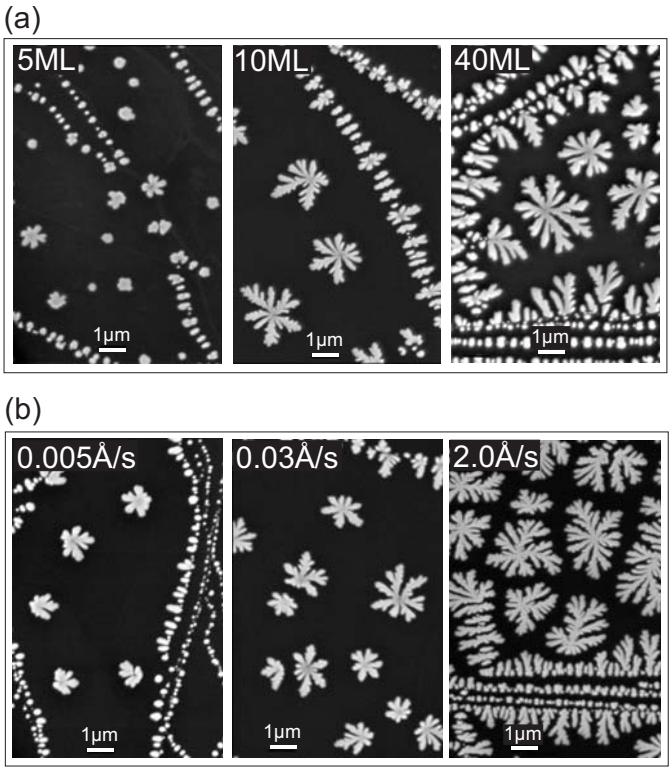

Fig. 1. Representative SEM micrographs of the evolution of surface morphology with: (a) increasing coverage (flux is held constant at 0.03 Å/s), (b) increasing flux (coverage is held constant at 10 ML).

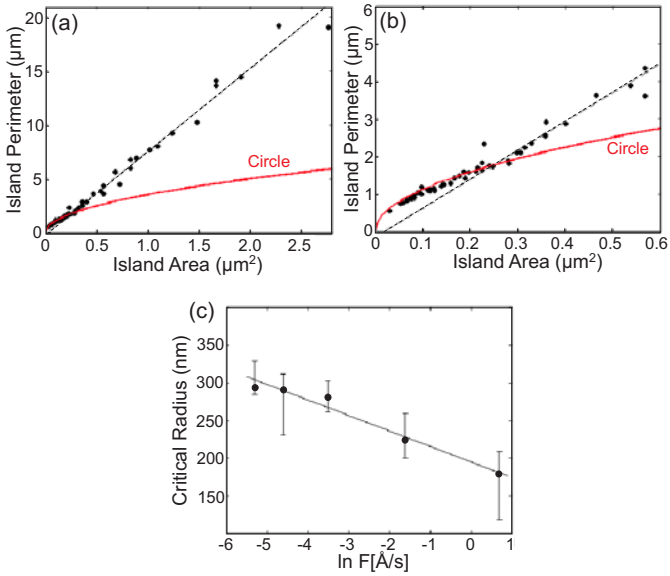

Fig. 2. (a) and (b) show plots of the island perimeter as a function of projected island area for a flux of 0.03 Å/s. The dashed line is a least squares fit to the data points, and the solid curve plots the dependence of a circle's circumference on its area, for comparison. (b) shows only data for islands smaller than 0.6 μm^2, to highlight the compact to branched transition in the data set. (c) Log-linear plot of the critical island radius as a function of increasing flux. Note that only islands found in regions of the sample which feature a low density of islands on large terraces (indicating a low defect density on the substrate) are included in the plots.

3 Results and discussion

3.1 Island morphology: an SEM investigation

Representative SEM images of the evolution of island morphology with increasing coverage are shown in Figure 1a, for a fixed flux of 0.03 Å/s. Island formation (Volmer-Weber [8] growth mode) is observed on the graphite surface, with the highest density of islands occurring along the HOPG step edges. The $\theta = 5$ ML image shows a mixture of small circular (compact) islands, and slightly larger islands featuring irregularities around their perimeter, with the most pronounced resulting in a fingered morphology. The fingering morphology becomes more dominant with increasing coverage as Mullins-Sekerka [9] type tip instabilities set in (as shown in the 10 ML and 40 ML images), resulting in large branched islands which cover an appreciable fraction of the substrate surface at 40 ML coverage.

Figure 1b shows the evolution of surface morphology with increasing flux, for a fixed coverage of 10 ML. As the flux is increased, the islands become progressively more branched, with the the high flux ($F = 2.0$ Å/s) environment producing aggregates which are similar to fractal islands found in many other systems [10–12]. It is also apparent that the islands project a greater surface area onto the substrate when the flux is increased, suggesting a reduction in height (this will be explored in Sect. 3.2).

It is clear that there is a transition from compact to branched morphologies with both increasing island size and particle flux. The island shape depends on two characteristic times [13]: the time between subsequent arrivals of Sb_4 clusters to the island boundary (arrival time, t_a), and the time required for an island to incorporate the cluster and rearrange into a thermodynamically favored compact shape (coalescence time, t_c). When $t_a > t_c$, compact shapes prevail. As the island grows larger, the coalescence time increases, inducing a cross-over from compact to branched shapes, where Mullins-Sekerka [9] type morphological instabilities prevail. As the deposition flux increases, the arrival time decreases. Consequently, the island has less time to rearrange (via processes such as edge diffusion) to a compact shape before more clusters arrive at its perimeter, and these instabilities set in earlier.

3.1.1 Analysis of island branching

Figure 2a shows a plot of the island perimeter as a function of increasing island area (flux is fixed at 0.03 Å/s), and includes data taken from multiple samples with different coverages to ensure a representative data set for this particular flux. The dashed line is a least squares fit to the experimental data points, and the solid curve shows

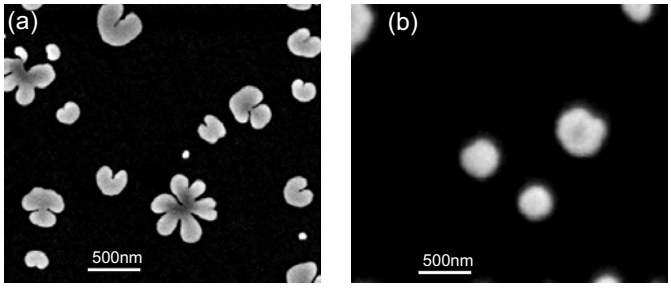

Fig. 3. SEM images of island nucleation on: (a) a defect contaminated substrate, (b) a relatively clean substrate. $\theta =$ 10 ML, $F = 0.03$ Å/s.

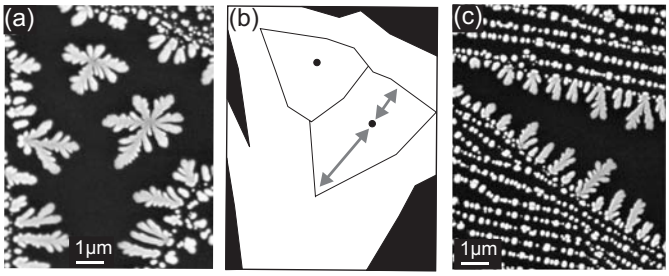

Fig. 4. The effect of competitive capture on the island morphologies. $\theta = 40$ ML, $F = 0.01$ Å/s. (a) SEM image showing two terrace nucleated islands. (b) Voronoi polygons for the two islands in (a). (c) Step edge decoration.

the dependence of a circle's circumference on its area (for comparison). Figure 2b shows the plot from Figure 2a, focusing on data for islands smaller than 0.6 μm^2. Initially the experimental data lies on the plot for a model circle, showing that the small islands are compact. At an island size of approximately 0.25 μm^2, the data departs from this curve, marking the transition to branched morphologies with increasing island size. The dashed line in both plots is a least squares fit to the data points which lie beyond this transition, and shows that the perimeters of the branched islands have a linear relationship to the island area for $A > 0.25$ μm^2.

Figure 2c shows a plot of the critical island radius for the compact to branched transition, as a function of flux. (as determined via the method described above for the $F = 0.03$ Å/s example, the error bars represent the spread in the data to both sides of the intersection between the linear fit and the model circle). The solid line is a least squares fit to the data. This plot shows that there is a distinct reduction in the critical island radius when the particle flux is increased, with values ranging between approximately 180 nm and 290 nm.

The values of the critical island radius plotted in Figure 2c only apply to islands nucleated on regions of the substrate with a low defect density (i.e. relatively clean HOPG). Figure 3 compares an an example of island nucleation on a substrate that was not heated sufficiently to remove adsorbed contaminants, (a) with nucleation on a correctly prepared (clean) substrate, (b). The morphology on the defect contaminated substrate is characterized by a higher density of irregularly shaped islands, many of them with crescent shapes. These islands are smaller than the critical island radius for this flux, which is 280 ± 20 nm from Figure 2c. Therefore it seems that surface contaminants effect the morphology of the islands, inducing the fingering morphology at significantly smaller island sizes.

Kaiser et al. [5] report a critical island radius of about 60 nm (and note that compact islands are never observed beyond this radius), which is significantly smaller than we present in Figure 2c. Their SEM images of compact islands feature a significantly higher island density than in our case, indicating the likelihood of nucleation on defect sites.

3.1.2 Competitive capture

The local flux surrounding an island varies depending on the proximity of neighboring islands which compete for capture of particles from the diffusion field (competitive capture). Figure 4a shows two terrace nucleated islands islands from a $\theta = 40$ ML, $F = 0.01$ Å/s sample. Figure 4b shows the capture zones (or Voronoi polygons [14]) for each of these islands. Any particle deposited within a particular capture zone has a maximum probability of contributing to the growth of the island nucleated within it (indicated by black dots). The two arrows in Figure 4b highlight that the length of the capture zone surrounding an island varies depending on the proximity of its neighbors.

Island branches tend to grow longer and more branched towards regions which are void of other islands, since there are more diffusing particles available (larger capture zones) and consequently a faster impingement rate to the branches' growth front. This is demonstrated by the centre island in Figure 4a, where the more branched island arm extends in the direction of the long arrow in Figure 4b.

Figure 4c shows a pronounced example of the effects of competitive capture. The structures nucleated along the closely spaced step edges in the image tend to feature compact morphologies, owing to their small capture zones. However, there is an increase in the diffusion field between the two widely spaced step edges in the centre of the image, which results in faster and less stable growth, and produces long branched morphologies.

3.2 3-Dimensional aggregation: An AFM study

3.2.1 Variation with coverage

Figure 5 shows two AFM images (in 3-dimensional plotting mode) of islands from a $\theta = 10$ ML, $F = 0.03$ Å/s sample. The images reveal height variances within individual islands, requiring that AFM cross-sections are taken at multiple locations to ensure a representative account of the 3-dimensional morphology.

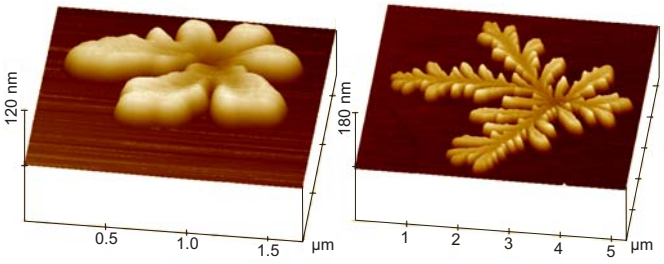

Fig. 5. AFM images of two antimony islands from a θ = 10 ML, $F = 0.03$ Å/s sample, note the scale change between the two images.

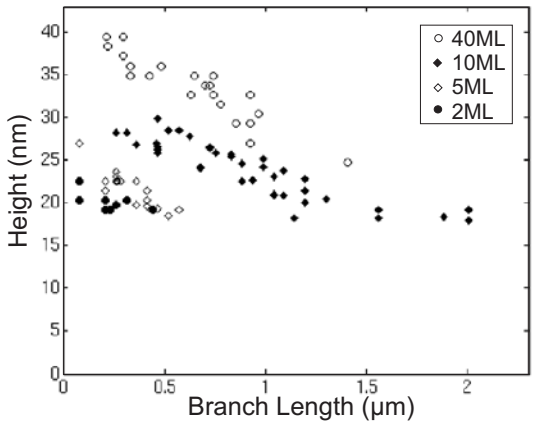

Fig. 6. Plot of the island branch height as a function of branch length, for various coverages (indicated by the legend). The flux is fixed at 0.03 Å/s.

Figure 6 shows a plot of the branch height (measured at the tip) as a function of the branch length for the coverages indicated by the legend (flux is fixed at 0.03 Å/s). The data for each coverage is taken from multiple islands, and in some cases multiple samples to ensure that the plot depicts a representative account of the island heights for this particular flux. It is apparent from Figure 6 that for any given coverage, longer branches tend to be flatter (which will be addressed in the next section). For this reason, the island heights are characterized in terms of branch length, rather than quoting a mean height to represent a given flux and coverage. Figure 6 also shows that the branch heights increase with increasing coverage. Note that the 2 ML and 5 ML data sets in this plot are taken from predominantly compact islands (since these dominate the low coverage samples), in these cases the branch length is taken as the radius of a circular island.

The increase in the general island heights with increasing coverage in Figure 6 shows that as deposition proceeds, a portion of the new material arriving to the growth front is transported upward, allowing island growth normal to the substrate. However, the majority of material contributes to lateral (2-dimensional) island growth. For example, the $\theta = 10$ ML data set in Figure 6 reveals island heights between 17–30 nm, and the 10 ML SEM image at the same flux in Figure 1a shows that the islands are typically greater than 1 μm in lateral diameter, giving an aspect ratio of order 0.02.

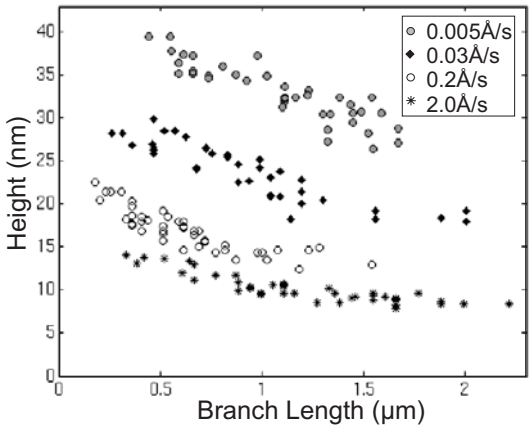

Fig. 7. Plot of the island branch height as a function of branch length, for various fluxes (indicated by the legend). The coverage is fixed at 10 ML.

3.2.2 Variation with flux

Figure 7 presents a plot of the branch height as a function of branch length for various fluxes (indicated by the legend), with the coverage fixed at 10 ML. The data points for each flux are taken from multiple islands and multiple samples. This plot shows that for each flux, the branches become flatter with increasing length, and it appears that the very long branches level off to some minimum height for each flux. Figure 7 also shows that that the islands become flatter with increasing deposition flux, confirming the qualitative observation from the SEM images in Figure 1b.

Increasing the particle flux reduces the available time for transport of particles from the perimeter to the top of the island (rearrangement to 3-dimensional morphologies), before the next particles arrive from the diffusion field and 'pin' the previous material in place. This accounts for the reduction in island height with increasing deposition flux demonstrated in Figure 7. The reduction in branch height with increasing length in Figures 6 and 7, is also consistent with the increased growth rate for longer branches (compared to their shorter counter-parts, as was discussed in Sect. 3.1.2), allowing less time for 3-dimensional rearrangement.

Figure 8 shows a typical example of the effect of competitive capture of the diffusion field on the height profile. The AFM image shows two small islands nucleated close to each other, with an absence of other islands in their vicinity. The accompanying height profile taken through the horizontal line in the image, reveals that the sides of the islands facing each other are taller than other parts of the islands. The capture zone for diffusing particles is significantly reduced between the two islands, resulting in slower growth, and consequently a taller morphology.

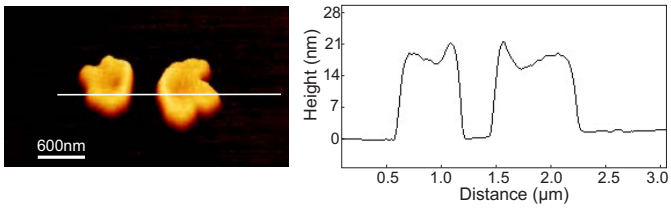

Fig. 8. The effect of competitive capture of the diffusion field on the island height profiles, $\theta = 5$ ML, $F = 0.03$ Å/s. Left: AFM image, with the position of a height cross-section indicated by the horizontal line. Right: height cross-section.

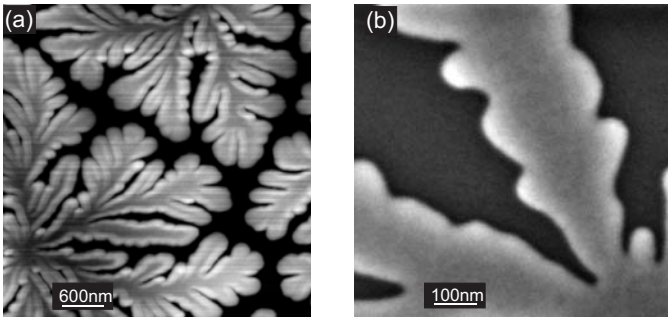

Fig. 9. Images demonstrating the build up of material around the perimeter of the island branches. (a) AFM image, $\theta = 40$ ML, $F = 2.0$ Å/s. (b) Field-emission SEM image $\theta = 10$ ML, $F = 0.03$ Å/s.

3.2.3 Island perimeters

In many of the AFM scans, a build up of material was found to exist around the island perimeters. Figure 9a shows a particularly pronounced example of the effect, where the branches have an increase in grey scale intensity around their edges, indicating an increase in height. Figure 9b shows a field-emission SEM image from a different sample with different deposition parameters. The increased brightness around the edges of the branches is again present, excluding the possibility of this feature being attributed to an AFM tip effect.

At the end of deposition, $t_a \rightarrow \infty$ since the diffusion field is diminished when the last clusters arrive to the islands' growth front. It seems likely that this allows for more 3-dimensional rearrangement of material during the final stages of island growth, leading to the build up of material around the edges of the fingered structures.

Figure 10 shows representative AFM images and height profiles for two islands with 10 ML coverage, deposited at $F = 0.03$ Å/s (a), and $F = 0.005$ Å/s (b). The height profile for the higher flux example clearly shows the elevated height at the branch edges, while this feature is absent in the profile from the low flux island. A low flux growth environment allows the aggregation of taller (more thermodynamically favorable) islands, which likely reduces tendency for further upward migration of material at the end of deposition.

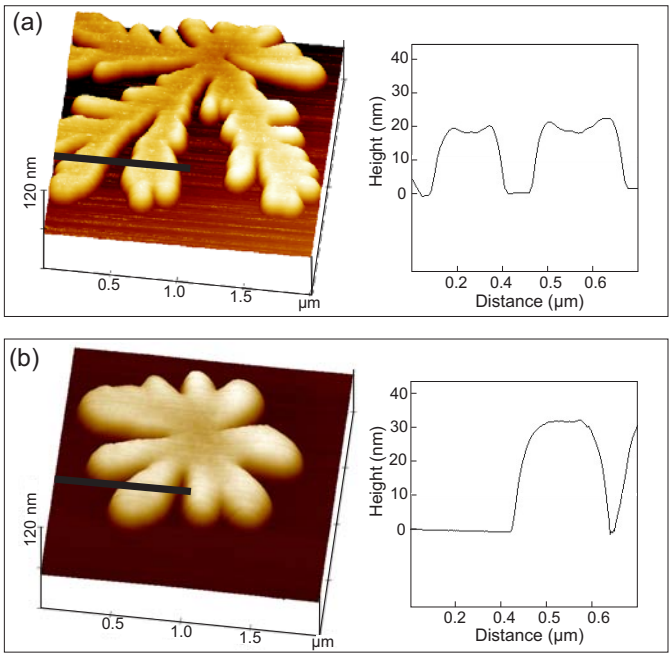

Fig. 10. 3-Dimensional AFM images and height profiles for islands with 10 ML coverage. (a) $F = 0.03$ Å/s, the height cross-section (right) shows elevated heights at the edges of the branches. (b) $F = 0.005$ Å/s, the height cross-section (right) does not feature the elevated height at the island edges.

4 Conclusion

With increasing particle flux, the critical island radius for the transition from compact to branched morphologies reduces from ∼290 nm ($F = 0.005$ Å/s) to ∼180 nm ($F = 2.0$ Å/s), on the large graphite terraces. The proximity of neighboring islands also effects the morphology, since the local growth rates (and hence time for rearrangement) are altered due to competitive capture of the diffusion field. Consequently, flatter and more branched islands are found to extend toward regions where there is an absence of other islands.

The aggregation of antimony islands on HOPG represents a classic system where the interplay between kinetics and thermodynamics determines the 3-dimensional morphology. Low fluxes shift the balance towards more thermodynamically favorable compact and taller structures, while higher fluxes increase the kinetic dominance, resulting in flatter and more branched morphologies.

We are grateful to B. Kaiser (Darmstadt Technical University) for useful discussions and early help in establishing this project.

References

1. Z. Zhang, M. Lagally, Science **276**, 377 (1997)
2. *Metal Clusters at Surfaces*, edited by K.-H. Meiwes-Broer (Springer, Berlin, 2000)

3. B. Yoon, V. Akulin, P. Cahuzac, F. Carlier, M. de Frutos, A. Masson, C. Mory, C. Colliex, C. Bréchignac, Surf. Sci. **443**, 76 (1999)
4. J. Le Roux, Ph.D. thesis, Université Paris-Sud, 2002
5. B. Kaiser, B. Stegemann, H. Kaukel, K. Rademann, Surf. Sci. **496**, L18 (2002)
6. B. Stegemann, C. Ritter, B. Kaiser, K. Rademann, J. Phys. Chem. B **108**, 14292 (2004)
7. J. Mühlbach, P. Pfau, E. Recknagel, K. Sattler, Surf. Sci. **106**, 18 (1981)
8. M. Volmer, A. Weber, Z. Phys. Chem **119**, 277 (1926)
9. W. Mullins, R. Sekerka, J. Appl. Phys. **34**, 323 (1963)
10. E. Sharon, M. Moore, W. McCormick, H. Swinney, Phys. Rev. Lett. **91**, 205504 (2003)
11. R. Hwang, J. Schroder, C. Gunther, R. Behm, Phys. Rev. Lett. **67**, 3279 (1991)
12. M. Conti, B. Meerson, P. Sasorov, Phys. Rev. Lett. **80**, 4693 (1998)
13. C. Bréchignac, P. Cahuzac, F. Carlier, C. Colliex, M. de Frutos, N. Kebaili, J. Le Roux, A. Masson, B. Yoon, Eur. Phys. J. D **16**, 265 (2001)
14. P. Mulheran, J. Blackman, Philos. Mag. Lett. **72**, 55 (1995)